ADVANCES IN PHYSICS AND APPLICATIONS OF 3D MAGNETIC PERTURBATIONS ON THE J-TEXT TOKAMAK

Nengchao Wang[1,*], Y. Liang[1,2,3,*], Yonghua Ding[1], Zhongyong Chen[1], Zhipeng Chen[1], Zhoujun Yang[1], Donghui Xia[1], Wei Zheng[1], Wei Yan[1], Da Li[1], Zhonghe Jiang[1], Lu Wang[1], Bo Rao[1], Qiming Hu[4], Xiaolong Zhang[5], Junli Zhang[1], Xixuan Chen[1], Xin Xu[1], Tao Xu[1], Xianli Xie[1], Zhuo Huang[1], Feiyue Mao[1], Dongliang Han[1], Jianchao Li[5], Tong Wang[1], Linzi Liu[1,6], Ruihai Tong[1,6], Zhifang Lin[1,7], Yunong Wei[1], Nianheng Cai[1], Yuejiang Shi[8], Yaping Zhang[1], Weixin Guo[1], Xiaoqing Zhang[1], Peng Shi[6], Zhifeng Cheng[1], Ping Zhu[1], Minghai Liu[1], Shaoxiang Ma[1], Yong Yang[1], Chuan Li[1], Li Gao[1], Zhijiang Wang[1], Ming Zhang[1], Kexun Yu[1], Xiwei Hu[1], Q. Yu[9], K W Gentle[10], Yuan Pan[1] and the J-TEXT Team[†]

[1]International Joint Research Laboratory of Magnetic Confinement Fusion and Plasma Physics (IFPP), HUST, China; [2]FZJ, Germany; [3]ASIPP, China; [4]PPPL, US; [5]SZU, China; [6]SWIP, China; [7]JSNU, China; [8]ENN, China; [9]IPP Garching, Germany; [10]IFS, UTEXAS, US.

Corresponding Author: Nengchao Wang, wangnc@hust.edu.cn; Y. Liang, y.liang@fz-juelich.de

Abstract

As of a long-term research program, the J-TEXT experiments aim to develop fundamental physics and control mechanisms of high temperature tokamak plasma confinement and stability in support of success operation of the ITER and the design of future Chinese fusion reactor, CFETR. In the past two years, three major achievements have been made on J-TEXT in supporting for the expanded operation regions and diagnostic capabilities, i.e. the 105 GHz/500 kW/1 s ECRH system, the poloidal divertor configuration and upgrades of several new diagnostics. Especially, the 400 kW ECW has also been successfully injected into the diverted plasma. The locked mode (LM), especially the 2/1 LM, is one of the biggest threats to the plasma operation, since it can lead to major disruption. It is hence important to study its formation and control. Both the thresholds of 2/1 and 3/1 LM are observed to vary non-monotonically on electron density. The electrode biasing (EB) was applied successfully to unlock the LM from either a rotating or static RMP field. In the presence of 2/1 LM, three kinds of standing wave (SW) structures have been observed to share a similar connection to the island structure, i.e. the nodes of the SWs locate around the O- or X- points of the 2/1 island. The control and mitigation of disruption is essential to the safe operation of ITER, and it has been systematically studied by applying RMP field, MGI and SPI on J-TEXT. When the RMP induced 2/1 LM is larger than a critical width, the MGI shutdown process can be significantly influenced. If the phase difference between the O-point of LM and the MGI valve is +90° (or -90°), the penetration depth and the assimilation of impurities can be enhanced (or suppressed) during the pre-TQ phase and result in a faster (or slower) thermal quench. During the MGI shutdown process, the runaway electron (RE) generation can be suppressed once n_e is larger than a critical threshold. This n_e threshold can be reduced by applying RMP field. A secondary MGI can also suppress the RE generation, if the additional high-Z impurity gas arrives at the plasma edge before TQ. When the secondary MGI has been applied after the formation of RE current plateau, the RE current can be dissipated, and the dissipation rate increases with the injected impurity quantity, but saturates with a maximum of 28 MA/s.

1. INTRODUCTION AND TECHNICAL IMPROVEMENTS

As of a long-term research program, the J-TEXT [1, 2] experiments aim to develop fundamental physics and control mechanisms of high temperature tokamak plasma confinement and stability in support of success operation of the ITER and the design of future Chinese fusion reactor, CFETR. Recent research has highlighted the significance of the role that non-axisymmetric magnetic perturbations, so called 3D magnetic perturbation (MP) fields, play in fundamentally 2D concept, i.e. tokamak. In this paper, the J-TEXT results achieved over the last two years, especially on the impacts of 3D MP fields on magnetic topology, plasma disruptions, and MHD instabilities, will be presented.

In the past two years, three major achievements have been made on J-TEXT in supporting for the expanded operation regions and diagnostic capabilities, i.e. the electron cyclotron resonance heating (ECRH) system, the poloidal divertor configuration and upgrades of several new diagnostics.

---

[*] Authors to whom any correspondence should be addressed.

[†] See appendix.

1.1. Successful operation of ECRH systems

In order to improve the plasma parameters and broaden the operation range of J-TEXT tokamak, a 105 GHz/500 kW/1 s ECRH system has been under development since 2017. The key microwave component in the ECRH system is a 105 GHz/500 kW/1 s GYCOM gyrotron. Considering the toroidal field of J-TEXT, this system is designed to work at the X2 mode for plasma heating and current drive. Figure 1 shows the layout of the ECRH system on the J-TEXT tokamak.

Based on the requirements for practical application, the detailed design for some of components in the ECRH system are accomplished. The launcher is expected to inject the microwave power generated by the gyrotron to the desired position in the plasma, the quasi-optical design and rotating mechanism design are of great significance. The launcher can be rotated at the toroidal and poloidal directions independently and the scanning range is no less than 20° [3], as shown in Figure 1 (b). To match the electron cyclotron wave with the plasma efficiently, two polarizers including a linear polarizer and an elliptical polarizer are designed. The linear polarizer is mainly used to change the rotation angle of the wave, while the ellipticity of the wave is regulated by the elliptical polarizer [4]. Besides, to ensure the safe operation of the system, two types of fast protection units are designed. One is the overvoltage and overcurrent fast protection unit, and the other is the arc fast protection unit [5]. The ECRH system has been successfully commissioned at the beginning of 2019. Figure 2 displays one example with 350 kW ECRH injected during the first commission phase. Currently, the ECW with a power of more than 400 kW has been successfully injected into the plasma, increasing the core electron temperature from 0.9 keV up to around 1.5 keV.

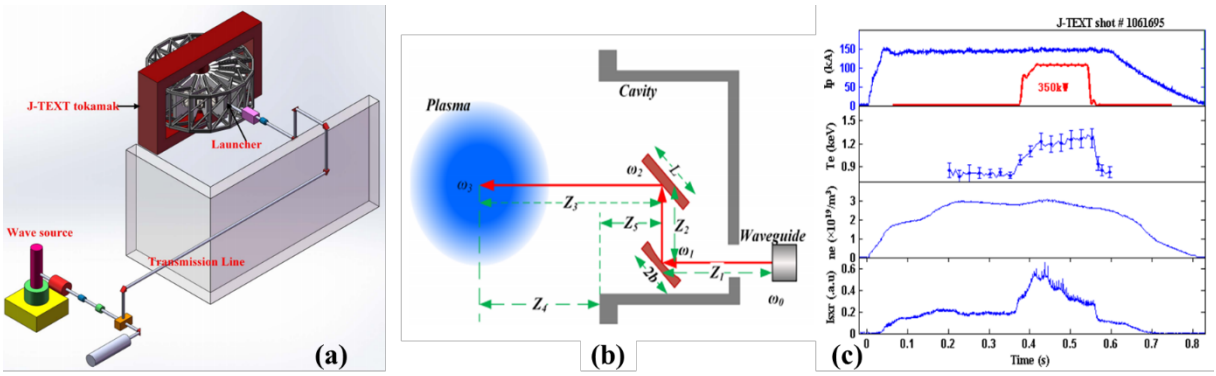

Figure 1 (a) Layout of the 105 GHz ECRH system on J-TEXT. (b) Schematic of the ECRH launcher. The microwave is reflected by focusing mirror and steering mirror in turn. (c) A typical discharge with 350 kW ECRH. [3]

1.2. Operation of the poloidal divertor configuration

The operation with a poloidal divertor is of great importance for impurity exhaust and confinement improvement in a tokamak. After the reconstruction [2], J-TEXT retains the TEXT-U divertor coils [6] in the high-field side (HFS). These coils can form four baseline divertor configurations with X-point(s) in the HFS, i.e. mid-plane single-null (MSN), double-null (DN), upper single-null (USN) and lower single-null (LSN). The operation of J-TEXT in the divertor configuration was put forward in 2016. Along with the establishment of power supplies for divertor coils [7], the construction of relevant diagnostics [8, 9] and installation of the divertor target in the HFS, the plasma operation in the divertor configuration was tested from the end of 2018.

The special MSN divertor configuration has been realized for the first time in J-TEXT [10], as shown in Figure 2 for an example. When the plasma current I_p reaches its flattop, the horizontal position of plasma, dx, is pushed outward for 2 cm with respect to the routine center in the limiter configuration (Figure 2(b)). Moving plasma towards the low field side (LFS) allows a better stability during the transition to MSN, according to the in-out instability analysis [10]. Once dx reaches 2 cm at 0.25 s (Figure 2(e1)), the divertor coil current I_{DV} starts to rise for 0.2 s and reaches its flattop for a duration of 0.1 s (Figure 2(c)). With the ramping of I_{DV}, clear plasma shaping in the HFS mid-plane is visible (Figure 2(e2)), and then the X-point is pushed into the vacuum vessel forming the divertor configuration at 0.446 s, as indicated by the sharp increase of floating potential measured in the HFS mid-plane (Figure 2(d)) and the reconstructed flux surface in Figure 2(e3). A successful MSN divertor configuration (Figure 2(e4)) is maintained for 0.1 s. Figure 3(a) displays a typical image of the MSN operation.

The 400 kW ECW has also been successfully injected into the diverted plasma. A clear increase of the core electron temperature is observed, and the increased heat flux towards the SOL and the upper/lower strike points leads to intensive recycling and serious release of impurity, as observed from the increase of visible light emission shown in Figure 3(b).

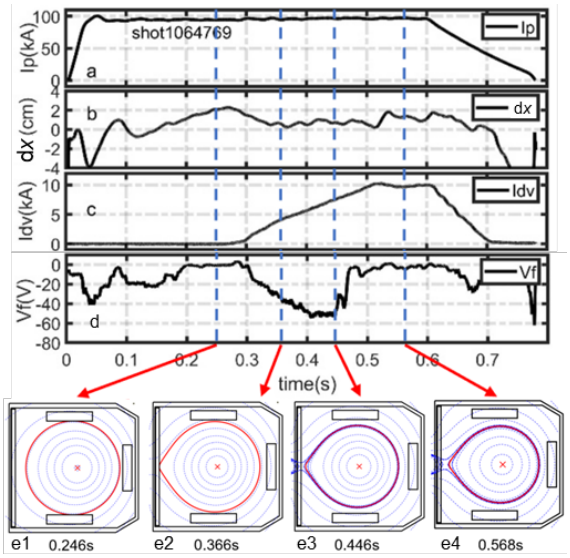

*Figure 2 Typical divertor configuration discharge on J-TEXT, with I_p = 100 kA, B_T = 2 T, n_e = 1.5*10^{19}m^{-3}. The time evolution of (a) plasma current, (b) plasma horizontal displacement, (c) divertor coil current, (d) floating potential measured on the mid-plane divertor target. (e1-4) The reconstructed flux surface contours at four time slices.*

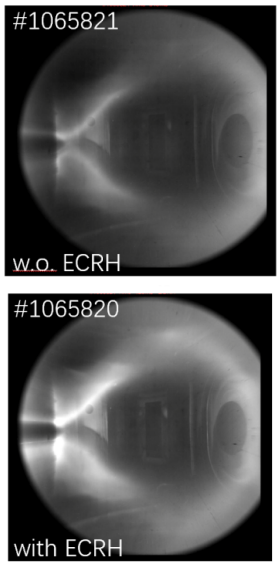

Figure 3 The visible emission photos for two MSN discharges with and without ECRH.

1.3. Upgrade of diagnostics

Several diagnostics have been developed and upgraded on J-TEXT. A new 256-channel electron cyclotron emission imaging (ECEI) system has been installed on J-TEXT at the end of 2019 [11]. It is an innovative design which first adopts lots of digital control components to realize the intelligent remote control [12, 13]. The J-TEXT ECEI system consists of two receiving antenna arrays for different depth measurements at the same toroidal position, while operating in W-band (75-110 GHz) and F-band (90-140 GHz). Each antenna array has 16 independent vertical receivers covering 8 radial detection volume at different poloidal viewing. A multi-channel Doppler Reflectometer (DR) system has been developed on J-TEXT. It has two sets of 4-channel fixed frequency unit and a 4-channel tunable frequency unit which cover U-band and Q-band frequency. The DR system can provide the information for plasma turbulence research, such as the density fluctuation, poloidal rotation, radial electric field and so on [14]. The Vacuum Ultraviolet (VUV) spectroscopy system on J-TEXT has also been upgraded to improve the temporal resolution for transport study. A micro-channel plate (MCP) has been added to transmit the VUV light (30-200 nm) to visible light for acquisition by the Electron Multiplying Charge Coupled Device (EMCCD). Its temporal resolution is improved from 40 ms to about 2 ms [15]. These diagnostics will support the future researches on the disruption physics, the turbulence, and especially the interplay between global MHD modes and turbulence.

2. PROGRESS ON MHD RESEARCHES

The locked mode (LM), especially the 2/1 LM, is one of the biggest threats to the plasma operation, since it can lead to major disruption. It is hence of great importance to estimate the threshold of its formation and to control it with high reliability. The locked mode is formed due to either the locking of a rotating tearing mode (TM) to the resonant component of error field or the penetration of external resonant magnetic perturbations (RMPs). The latter is of great concern to the low density start-up phase of ITER. A non-monotonic density dependence is

observed for the 2/1 LM threshold [16] on J-TEXT. Following the previous achievement of the LM unlocking by rotating RMP [17], the electrode biasing (EB) was applied successfully to unlock the LM from either a rotating or static RMP field [18]. In the presence of 2/1 LM, three kinds of standing wave (SW) structures [19, 20, 21] have been observed to share a similar connection to the island structure, i.e. the nodes of the SWs locate around the O- or X- points of the 2/1 island.

2.1. Density scaling of the RMP penetration threshold

It is previously found in J-TEXT that the 2/1 RMP penetration threshold, $b_{r,th}^{2/1}$, increases approximately with $n_e^{0.5}$ in the density range of (0.7 ~ 2.7)*10^{19} m^{-3} [22]. The density scaling coefficient, α_n being around 0.5, is lower than those observation of $\alpha_n \sim 1$ in many other devices [23], however $\alpha_n \sim 0.5$ is also observed later on EAST [24]. With the installation of 12 new in-vessel RMP coils (2-turns) in 2017 [1], larger RMP amplitudes can be provided. The density dependence of $b_{r,th}^{2/1}$ is then extended toward higher density (blue dots, Figure 4(a)). It is found that once n_e is larger than a critical value, the penetration threshold dramatically decreases with further increase of n_e [16]. It is noted that the non-monotonic density dependence of $b_{r,th}^{2/1}$ is also observed in KSTAR and DIII-D [25]. The DIII-D case might be explained by the similar non-monotonically dependence of local density at $q = 2$ (n_e^{q2}) on the core line-averaged density $\bar{n}_e$, while $n_e^{q2} \propto \bar{n}_e^{0.68}$ on J-TEXT.

The toroidal rotation at the $q = 2$ resonant surface, which plays an important role in the 2/1 RMP penetration yet being not included in the empirical scaling, also shows a similar non-monotonic density dependence (red diamonds, Figure 4(a)) on J-TEXT as that of $b_{r,th}^{2/1}$. The multiple linear regression provides a scaling in the form of $b_{r,th}^{2/1} \propto n_e^{-0.18\pm0.04} f_0^{1.04\pm0.25}$, where f_0 (the initial MHD frequency) is experimentally estimated by $f_0 = 0.3V_\phi + 8.5$ [26]. This scaling reveals that there is only a weak or even no dependence of the 2/1 RMP penetration threshold on the density and a linear dependence on the plasma rotation. This result is not only important for the prediction of error field tolerance in fusion devices, but also opens a question on the role of density in the forced magnetic reconnection process in magnetized plasmas.

It would be interesting to study whether the density dependence of $b_{r,th}^{2/1}$ remains at other rational surfaces. The previous scaling for the 3/1 RMP penetration in the low density range of (0.6 ~ 1.5)*10^{19} m^{-3} [27] is extended to 4.5*10^{19} m^{-3} by using the 2-turns RMP coils (Figure 4(b)). It is found that $b_{r,th}^{3/1}$ also show a similar non-monotonically dependence on density [28], and the roll-over density is at around 3*10^{19} m^{-3}. The variation of plasma rotation at q= 3 surface will be compared in detail in the future. The penetration of 2/2 RMP [29] requires all the 24 RMP coils and their currents approach to the maximum available value. So the 2/2 RMP penetration is currently observed only at fairly low q_a (= 2.5~2.8) and low density (< 2*10^{19} m^{-3}), which is lower than the roll-over density of the 2/1 RMP penetration [16]. Figure 4(c) shows a linear dependence of $b_{r,th}^{2/2}$ on density. It is not yet clear how $b_{r,th}^{2/2}$ would change at higher density, since the density dependence of V_ϕ might be difference in the core (q = 1) and the edge (q = 2 or 3) plasma.

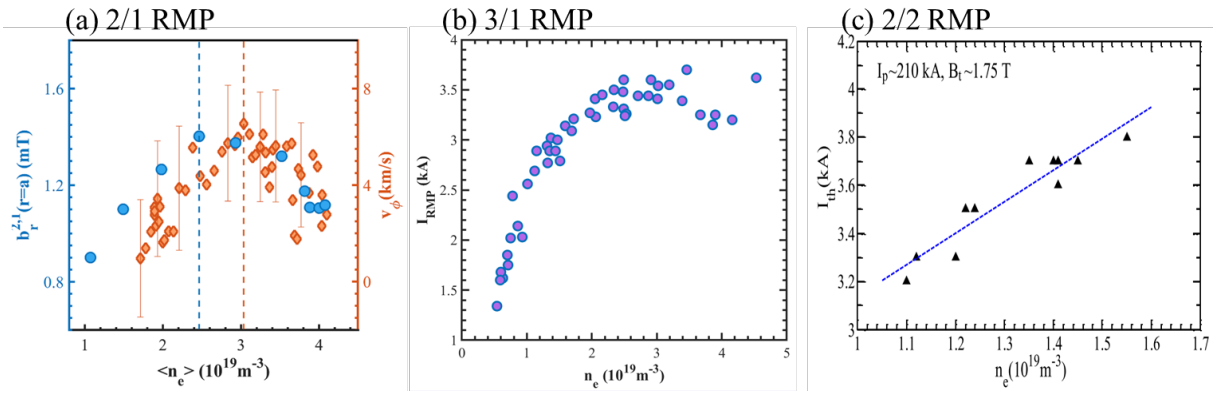

Figure 4 Density scaling of the penetration threshold of RMP, with dominant resonant component at m/n = (a) 2/1 [16], (b) 3/1 and (c) 2/2 [29].

2.2. Locked mode control via electrode biasing

The external momentum input has been applied to unlock the locked modes either by rotating RMP [17] or by NBI [30]. The EB is also an efficient method to modify the plasma rotation, and it is found to be capable of

increasing or decreasing the TM frequency with positive or negative biasing on J-TEXT [31]. Recently, EB is applied to study its impact on locked modes, and it successfully unlocks the LM [18] from either a static or rotating RMP field as summarized in Figure 5. The 2/1 RMP field is applied to lock the TM and to maintain its locking status for 200 ms (#1061441, blue lines). As the first demonstration of unlocking, the RMP amplitude is reduced to a smaller amplitude after locking, so that locked mode won't lead to major disruption. When the EB is applied at 0.39 s in #1061442 (red), the phase difference (Figure 5(b)) between the LM and the 2/1 RMP increases in the ctr-I_p direction and the LM amplitude (Figure 5(c)) decreases. The LM is unlocked when the phase difference reaches about -95°. The mode frequency then quickly increases from 0 to about 3 kHz, followed by a slow increase to about 4.5 kHz. Statistical analysis shows that the LM is easier to be unlocked with stronger EB current or weaker LM amplitude.

Remarkably, the synergy effect of the EB and the RMP field can suppress the unlocked mode completely. With larger EB current in #1061447, the LM is unlocked earlier and it decays away after the unlocking. The mode frequency before its suppression is around 6 kHz, which is smaller than 7 kHz in the TM suppression cases with only EB [31]. If the negative EB is applied before the TM being locked to external static RMP, it can stop the mode locking process by abruptly increasing the TM frequency and lead to the suppression of TMs (# 1045120). The external momentum input from negative EB might counteract the braking effect of RMP, and hence the suppression effect of RMP on TM is possible at lower TM frequency, compared to that reported previously for RMP alone [32].

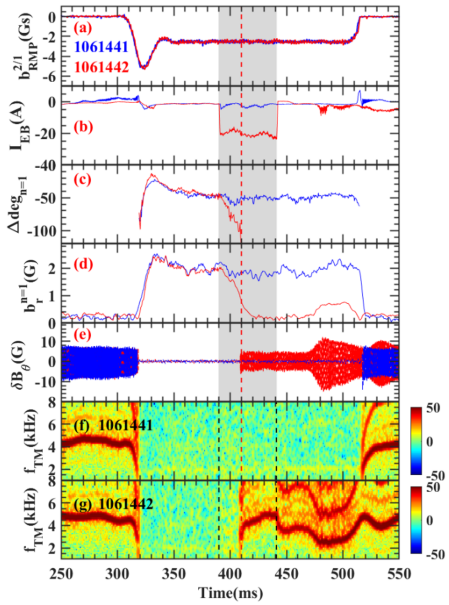

Figure 5 Unlocking of locked mode by EB [18]. Time evolutions of (a) the 2/1 component RMP amplitude, (b) EB current, (c) the phase difference between n = 1 locked mode and 2/1 RMP, (d) locked mode amplitude, (e) high frequency component (>0.5 kHz) of the poloidal magnetic perturbation (δB_θ), (f) and (g) the frequency spectrum from Mirnov probes showing the 2/1 mode frequency for shots 1061441 and 1061442. The shaded region shows the time period of applying EB. The red dashed line shows the time of mode unlocking for shot 1061442.

2.3. Standing waves in the presences of magnetic islands

Standing waves (SWs) have been widely observed in tokamak plasmas. In the J-TEXT experiments, three kinds of SW structures have been observed in the presence of large 2/1 magnetic islands, which can be either rotating at a few kilohertz or locked to the error field/RMP.

The first SW is identified to be the forced oscillation of the island phase [19] due to the application of a RMP field rotating at a few kHz (e.g. 1~6 kHz). Figure 6(a) and (b) displays an example where a 6 kHz rotating RMP is applied to a plasma with slowly rotating 2/1 TM. The rotating RMP induces an EM torque on the TM and leads to the phase oscillation of TM, $\delta\xi_{TM}$. The plasma responses to rotating RMP equal to the product of $\delta\xi_{TM}$ and the poloidal gradient of the plasma parameters, e.g. $\partial b_\theta^{2/1}/\partial\theta$ or $\partial T_e/\partial\theta$. Since $b_\theta^{2/1}$ has a maximum or minimal at the O- or X- point, the magnetic response δb_θ is around 0 at the O-/X- points, and changes sign on the two sides of O-/X- points. This then forms the observed SW structure, which have nodes around the O-/X- points, as shown in Figure 6(a). The T_e response at 6 kHz were zero or minimal when $\partial T_e/\partial\theta \sim 0$, i.e. inside the magnetic island, or outside the magnetic island but at the same poloidal positions as the O-/X- points.

The second kind of SWs is the so called Beta-induced Alfvén Eigenmodes (BAEs) [20] at 20 ~ 50 kHz observed with a locked or rotating magnetic island. BAEs have been widely observed with counter-propagating waves, and form SW structure in the island rest frame [33, 34]. It is found in J-TEXT that the nodes of BAEs also locate at the O-/X- points of the magnetic island, as shown in Figure 6(c) and (d). This feature is also found later in EAST [35].

The formation of BAEs with a SW structure hasn't been yet understood experimentally. It is noted that the spontaneously emerging BAEs and the artificial SWs induced by rotating RMP share a similar connection to the island structure, i.e. the nodes of the SWs locate around the O- or X- points of the 2/1 magnetic island. This connection might be a key to understand the BAEs. Moreover, a third SW [21] has been observed to appear spontaneously at ~ 3 kHz without any external 3 kHz RMP field. It also has nodes around the O-/X- points, and preliminary analysis indicates that it might be due to the spontaneous oscillation of island phase at 3 kHz. Future comparison between the second SW, i.e. BAEs, and the third SW would be important to reveal the mechanism of their formation.

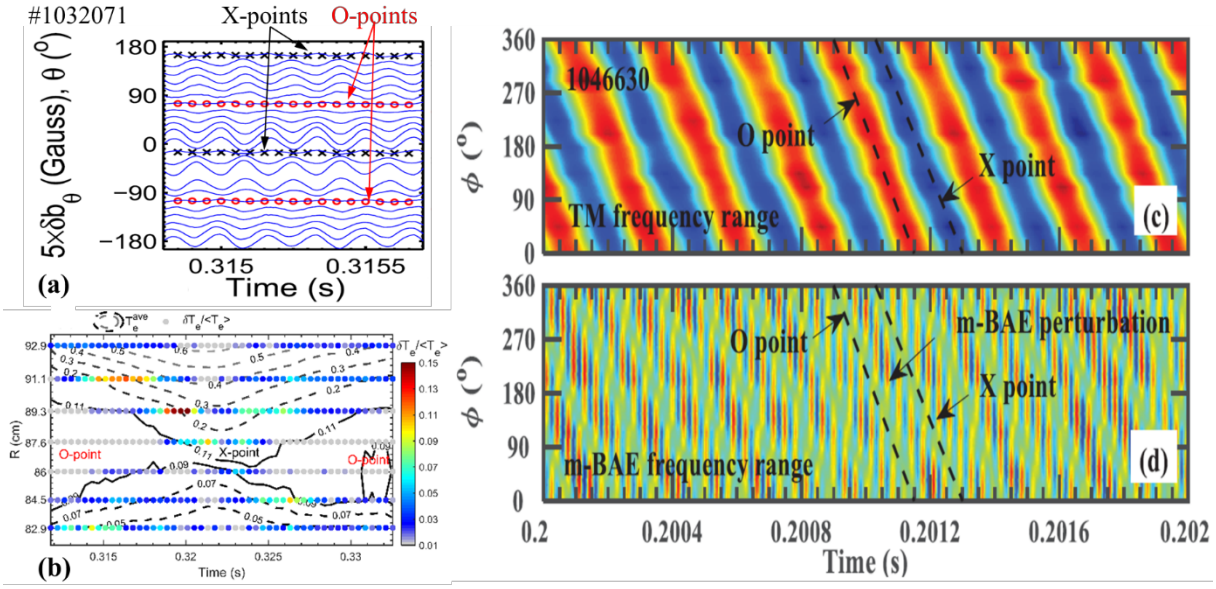

Figure 6 The two types of SW structures observed in J-TEXT. (1) The external 6 kHz rotating RMP induces a standing wave response [19] in both magnetic signals (a) and electron temperatures (b) in discharge #1032071. (2) The BAEs [20] show a SW structure with the nodes (d) locating at the O- and X- points (c) of the 2/1 magnetic island.

3. PROGRESS ON THE DISRUPTION CONTROL

Disruption is one of the urgent problems for future tokamaks in possibly causing heat loads, halo currents, and runaway electrons (REs). The control and mitigation of disruption is essential to the safe operation of ITER and future fusion reactors. In this section, we summarize the recent J-TEXT studies on the control of disruption triggered by the massive gas injection (MGI), focusing on the RE current suppression and dissipation. The RE suppression has been achieved by a secondary MGI [36,], the magnetic island seeded via the RMP penetration [37-40] or the magnetic energy transfer (MET) [41, 42], while the dissipation of RE plateau is studied by a secondary MGI [43, 44], a minus loop voltage [45] or the SPI [46].

3.1. Suppression of runaway current by MGI and MET

Massive impurity injection, e.g. MGI, is a feasible way to mitigate the disruption. Due to the limit of the impurity injection rate and the assimilation efficiency, single injection of impurity may not be sufficient to totally suppress RE generation in future large-scale devices. Large number of REs can form runaway currents and carry a large current fraction in the plasma current.

In order to suppress the formation of the runaway current, a secondary gas injection from an additional valve (MGI2) with a delay time to the valve of the disruption mitigation system (MGI1) is performed on J-TEXT [36], as summarized in Figure 7. If the time when the additional high-Z impurity gas arrives at the plasma edge, $t_{\text{arrival,MGI2}}$, is before the thermal quench (TQ), the runaway current (I_{RE}) can be significantly suppressed (magenta case) by weakening the primary RE generation, leading to a 90% reduction of the final formed I_{RE}. If $t_{\text{arrival,MGI2}}$ is during the current quench (CQ), I_{RE} can be partially suppressed (cyan case) by weakening the avalanche RE generation, leading to a 40%–80% reduction of the final formed I_{RE}.

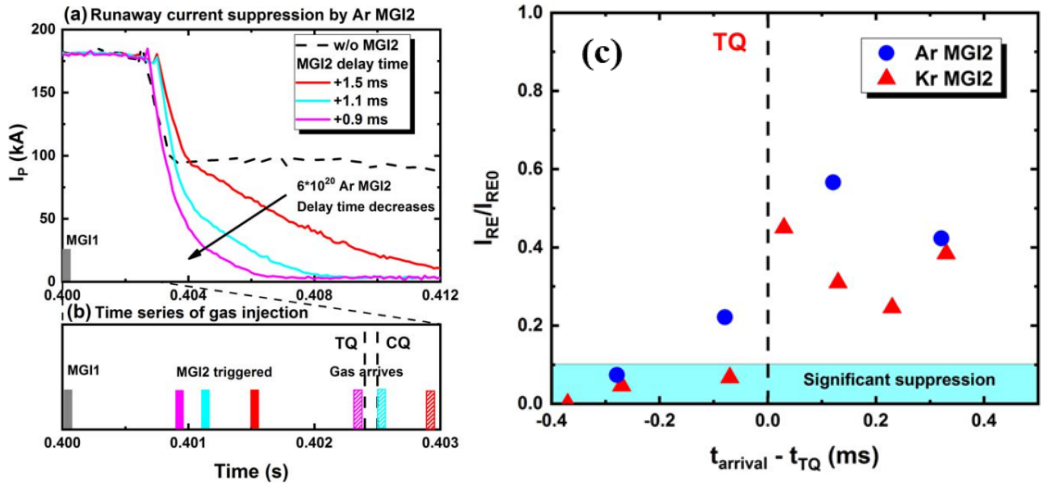

Figure 7 Runaway current suppression by a secondary MGI (MGI2) injected with different delay time after the first MGI, which triggers the disruption. (a) Time evolution of I_p decay caused by argon MGI2, (b) the time sequence of MGI1 trigger, MGI2 trigger, MGI2 arriving at plasma edge, TQ and CQ corresponding to (a). (c) The final runaway currents versus the relative MGI2 arrival times of the argon and krypton cases. [36]

An alternative path to suppress the RE generation would be to reduce the toroidal electric field, which is induced by the fast CQ and the large avalanche factor with high plasma current. Significant reduction of $E_{\parallel}$, or V_{loop}, and the suppression of RE have been achieved on J-TEXT by MET [41], as shown in Figure 8. The MET systems (Figure 8(a)) consists of the energy transfer coils (ETCs), which are strongly magnetically coupled with the plasma current, the energy absorbing unit (EAU) with a low resistance (10.3 mΩ), and a controlled switch, which connects the ETCs and EAU during the CQ. During the rapid plasma shutdown by MGI, a co-I_{p} current will be induced in ETCs and transfer the magnetic energy to EAU, which is outside the vessel. The MET system accelerates the CQ rate and reduces the toroidal electric field at the same time. With the increase of ETC current, the conversion fraction of runaway current is significantly reduced and the RE generation is completely suppressed when I_{ETCs} is above 6.5 kA (Figure 8(c)). The MET provides a new idea to transfer the magnetic energy and to suppress runaway current for disruption mitigation in future devices.

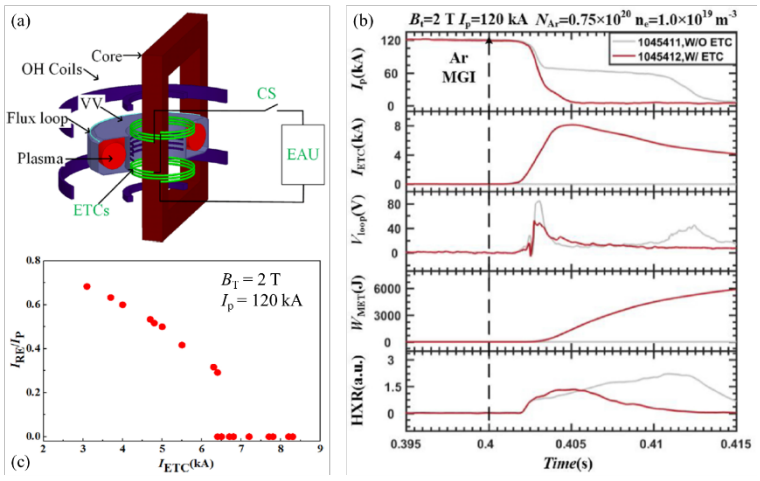

Figure 8 (a) Schematic of the MET system in J-TEXT. (b) Typical experimental result of runaway suppression by MET with I_{ETC} = 8 kA. (c) The influence of I_{ETC} on RE current fraction and suppression threshold.

3.2. Dissipation of runaway current

In case that RE suppression is not successful, a large fraction runaway current might form and hence is a great threat to the device. Developing a reliable method to dissipate RE current is also necessary. Several methods have been studied on J-TEXT in order to dissipate the larger I_{RE}.

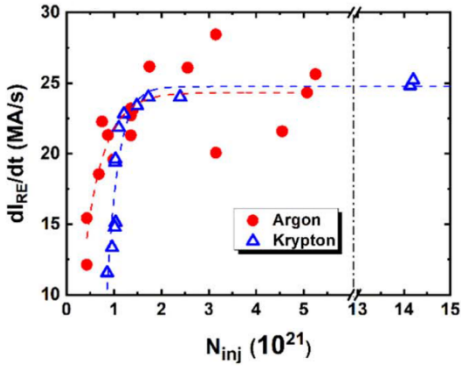

Figure 9. The runaway current dissipation rate versus the injected impurity quantity N_{inj}. [43]

The secondary MGI has been applied after the formation of RE current plateau to dissipate the RE current on J-TEXT [43]. It is found that the dissipation efficiency increases with the increase of injected impurity quantity, but saturates with a maximum of 28 MA/s when the injected impurity quantity exceeds 2×10^{21}, as shown in Figure 9. Analysis shows that the saturation of dissipation efficiency is caused by the decrease of impurity assimilation rate with the increase of total injected impurity quantity. The decrease of impurity assimilation rate may be caused by the saturation of impurity density growth rate during the short dissipation phase. A simple estimation also shows that the increase of internal inductance leads to the slowing down of the growth of runaway current dissipation rate during the runaway current decay phase. The results may have important implication for ITER disruption mitigation.

As another possible auxiliary method to dissipate the RE current, controlling the $E_{\parallel}$ via ohmic (OH) field has been performed to study the soft landing of RE current on J-TEXT [45]. Figure 10 displays a typical comparison among 3 discharges with different loop voltage. It is found that the RE current decrease faster with lower loop voltage. With optimized horizontal displacement control of the RE beam, the toroidal electric field has been scanned from 1.6 to -0.3 V/m during the RE plateau phase. It is found that when $E_{\parallel}$ is less than 7–12 times of the theoretical critical electric field, the decay of REs could be achieved. The dissipation rate by the OH field can reach a maximum value of 3 MA/s.

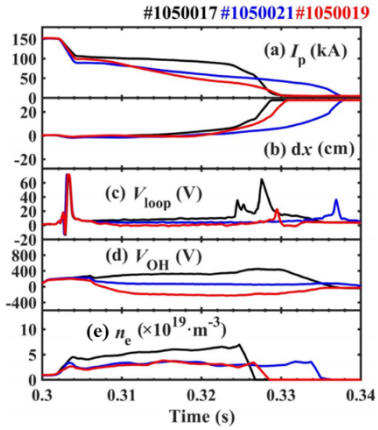

Figure 10 Evolution of RE currents in 3 discharges with different loop voltage. [45]

In addition to the above two method, the effect of SPI on runaway current dissipation in J-TEXT has been studied and compared with similar amount of Ar MGI injection. With the argon quantity of about 2.12×10^{21}, SPI dissipate the RE current at a rate of about 12 MA/s, slower than that with MGI (18 MA/s). Further details will be presented in this conference seperately [46].

3.3. Impact of RMP on the MGI triggered disruption

During the MGI shutdown process, the external applied RMP field might play various roles, either enhancing [47] or suppressing [48] the RE production, depending on the RMP amplitude. Recent studies on J-TEXT reveal more features of the impact of RMP on MGI triggered disruptions.

Without RMP, the RE generation can be suppressed once n_e is larger than a critical threshold. This n_e threshold is found to be reduced by applying a moderate RMP field, as shown in Figure 11 [37]. It is noted that in this case the RMP doesn't penetrate and hence no large locked island exists before the MGI. If the RMP is too strong or n_e is too low, the RE might also be suppressed although due to the impact of locked island [48].

Both the phase and width of the RMP induced 2/1 locked island are found to influence the MGI shutdown dynamics and RE generation. When the RMP induced 2/1 LM is larger than a critical width, the MGI shutdown process can be significantly influenced. If the phase difference between the O-point of LM and the MGI valve is +90° (or -90°), the penetration depth and the assimilation of impurities can be enhanced (or suppressed) during the pre-TQ phase and result in a faster (or slower) thermal quench [38]. Besides, the toroidal radiation asymmetry is observed to be worse in the case with LMs compared to the case without RMP.

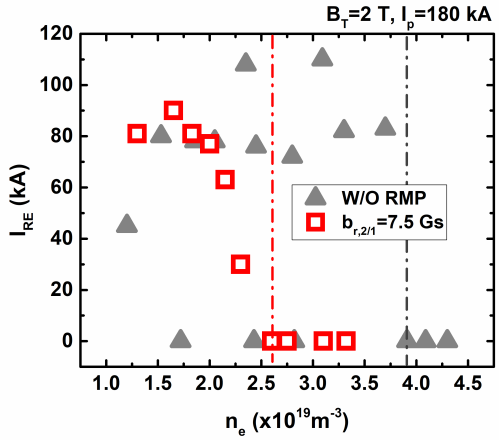

Figure 11 The formation of runaway current with different pre-disruption electron density for cases with 2/1 RMP (red squares) and without RMP (gray triangles). [37]

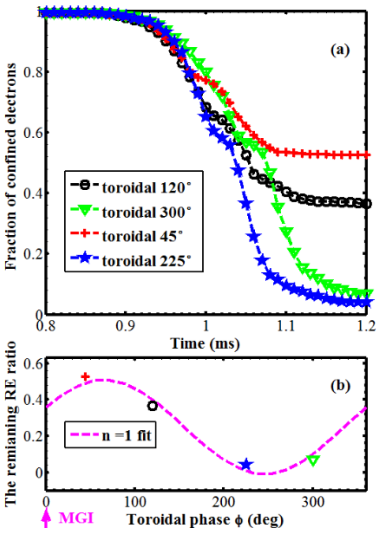

Figure 12 Effect of different phases of pre-seeded 2/1 locked islands on RE confinement. (a) Fraction of confined REs versus time (ms) for four island phases. (b) The dependence of the remaining RE ratio after the TQ on the toroidal phase of 2/1 islands.

Numerical studies on the role of RMP during MGI shutdown process are also performed with the 3D MHD code NIMROD. In the modelling, the locked islands are pre-seeded by the RMP penetration before MGI. Both the phase and amplitude of these locked islands are varied in the simulations.

It is found that the RE confinement is drastically affected by the magnetic island phase during the TQ phase, as shown in Figure 12. The remaining RE ratio shows an n = 1 dependence on the relative toroidal phase between the pre-seeded 2/1 island and the MGI valve (Figure 12 (b)) [39]. The optimized phase difference for runaway suppression is predicted to be toroidal 90º (ϕ_{MGI} - $\phi_{n=1}$). A discrepancy in the evolution of the flux surface among different toroidal phases of 2/1 islands has been found, which greatly depends on the magnetic perturbations induced in disruption. The RE confinement is also found to vary with the width of 2/1 locked island non-monotonically, as shown in Figure 13 [40]. Large enough pre-existing 2/1 magnetic islands can lead to strong magnetic perturbation and strong magnetic surface stochasticity to expel the REs. The critical width for the suppression of REs is to be 0.31 as the minor radius. The duration of magnetic perturbations $\delta B/B$(n = 1) (exceeding (4 to 6) × 10^{-3}) is a key for RE loss, and high amplitude of high n modes plays an important role in the RE loss.

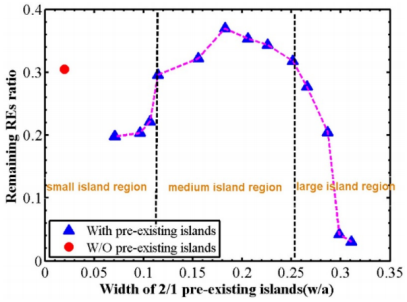

Figure 13 Dependence of the remaining RE ratio on the width of pre-seeded 2/1 locked islands.

Those results suggest that the 3D effect between the injected impurities and the 2/1 locked mode is important during the disruption mitigation process.

4. TURBULENCE AND TRANSPORT STUDY

4.1. Observation of non-local effects in ion transport channel

Following the previous observation of non-local transport (NLT) in multi-channel (electron temperature, particle, and momentum) [49], recent J-TEXT experiments reveals that the ion transport shows similar non-local response as the electron transport channel [50], owing to the improved temporal resolution of the ion temperature measurement to millisecond level. Very fast ion temperature decreases are observed in the edge, while the ion temperature in the core promptly begin to rise after the injection of cold pulse. Moreover, the cutoff density is also found for the ion non-local effect. The experimental observed density fluctuation in a high

frequency ranging from 500 kHz to 2 MHz is obviously reduced in the whole plasma region during non-local transport phase.

4.2. Electron thermal transport with ECRH

The electron thermal transport has been compared for the ohmic plasma and ECRH L mode plasma. It is found that the electron thermal diffusivity χ_e increases almost linearly with the ECRH power, as shown in Figure 14. The bandwidth of medium scale temperature fluctuation also become broaden as ECRH power increasing. With GENE simulation, it shows the low and medium scale turbulence translate from TEM and ITG mixed mode in ohmic plasma to pure TEM mode in ECRH plasma. The χ_e is also found to decrease as plasma density increasing in ohmic plasma, but almost no change for ECRH plasma. It indicates the ETG may dominate the electron heat transport in the ECRH plasma [51].

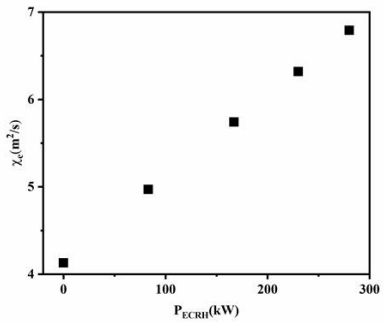

Figure 14 The electron thermal transport diffusivity (χ_e) versus different ECRH power.

4.3. Theoretical study on the turbulence

The intrinsic current driven by electromagnetic turbulence in pedestal region has been analytically investigated [52]. We found two types of intrinsic current driving mechanisms resulted from EM turbulence. The first type is the divergence of residual turbulent flux including a residual stress-like term and a kinetic stress-like term. The second type is named as residual turbulent source, which is driven by the correlation between density and parallel electric field fluctuations. This is analogous to the intrinsic rotation drive by EM turbulence [53, 54,]. However, the difference is that the intrinsic current density driven by the residual turbulent source is negligible as compared to that driven by the residual turbulent flux. Therefore, the modification of local current density could be significant. For EM electron drift wave in ITER pedestal region, there exists strong cancelation between non-adiabatic ES response and the non-adiabatic EM response, and thus the kinetic stress contributed by the adiabatic ES response of parallel electron pressure dominates the intrinsic current drive. This is different from the ES electron DW case. Therefore, the EM effects on turbulence driven intrinsic current density should be carefully considered in the future reactor with high ratio of electron pressure to the magnetic pressure and steep pressure profile. Moreover, the ratios of intrinsic current density driven by residual turbulent flux and by turbulent source to the bootstrap current density scales to $T_e^{3/4}T_i/n_e$ and T_eT_i/n_e, respectively [52].

In regard of the confinement of fast ions, we investigated the drift loss of fast ions induced by the combination of perturbed non-axisymmetric magnetic field and strong radial electric field in tokamak pedestal [55]. We use the single particle orbit model and neglecting the effects of finite Larmor radius and the width of the banana/transit orbit. The equations of motion of fast ions including the bounce/transit averaged radial drift and toroidal precession modified by the strong radial electric field have been derived. The strong radial electric field in pedestal significantly reduces the toroidal precession frequency of trapped fast ions, which plays an important role in the loss of trapped fast ions. Taking typical pedestal parameters in DIII-D corresponding to the case for ELM suppressed by RMP [56], we analyzed the parametric dependences of the drift loss: (1) passing fast ions can be well confined and will not escape from the plasma; (2) deeply trapped fast ions can lose from the plasma, but the loss range of parameters is narrow; (3) the drift loss time of trapped fast ions decreases with the increase of the energy of fast ions, the maximum amplitude of the RMP, the safety factor at the axis and the peaking factor of the plasma current density profile, and increases with the increase of the absolute value of the minimum radial electric field, the pitch angle-like parameter and the poloidal mode number of the RMP. This implies that the RMP makes the confinement of fast ions generated by perpendicular NBI weaker than that of fast ions generated by tangential NBI. Furthermore, we find that the drift loss time is smaller than the slowdown time by three orders of magnitude. Therefore, the drift loss of trapped fast ions induced by the RMP is an important loss mechanism for the DIII-D pedestal.

The parallel velocity shear (PVS) driven Kelvin–Helmholtz instability [57, 58] can be developed in magnetic fusion plasmas with high PVS, and it is theoretically found that the excitation of PVS turbulence is quite possible the partial reasons for experimental observation of the impurity accumulation in the present tokamaks with neutral beam injection (NBI) heating, for both the fully ionized light impurity (such as Be^{4+}, C^{6+}, Ne^{10+} from the intrinsic plasma-wall interaction or external injection) and heavy tungsten (W). While, increasing the electron density gradient is favorable for stabilizing the PVS mode and ease the accumulation of impurity,

because the inward impurity flux driven by PVS turbulence is significantly reduced [59]. Beside, role of PVS turbulence on the removal of helium ash is also investigated. When the density profile of helium ash is comparable or steeper than that of electrons (i.e., $R/L_{nz} \geq R/L_{ne}$, where L_{nz} and L_{ne} are the impurity and electron density gradient scale length, respectively, and R is the major radius), the normalized flux of helium ash is outward because the diffusivity is larger than inward convective velocity. Furthermore, isotopic effects (increasing the effective hydrogen isotope mass number) are favorable for expelling helium ash induced by PVS turbulence.

A mean field model, which is derived from the Hasegawa-Wakatani equation [60], is used to study the scale selection and feedback loops for the formation and sustainment of a staircase structure pattern. It is mainly found that the principle feedback loop is through the nonlinear dependence of mixing length on electron density gradient, rather than $\vec{E}\times\vec{B}$ shearing. When the zonal shear and mean shear are comparable, there will exist non-uniform staircase structure, and the minimal step scale is selected by competition between the initial density gradient (i.e., drive) and diffusive dissipation. Moreover, it is also found that finite turbulence spreading is necessary to form the staircase structure, while moderate enhancement of turbulence spreading will wash out this pattern. Then, we give the conclusion that the staircase-like structure in density (as well as in potential vorticity) is formed by self-sharpening of modulations, and the electron density gradient dependent mixing feedback is a natural route to enhanced confinement regimes, thus it acts as a candidate trigger mechanism for the L-H transition. More implications of these results have been discussed in the original paper [61].

5. SUMMARY AND OUTLOOK

Over the last two years, three major achievements have been made on J-TEXT in supporting for the expanded operation regions and diagnostic capabilities, i.e. the 105 GHz/500 kW/1 s ECRH system, the poloidal divertor configuration and upgrades of several new diagnostics. Especially, the 400 kW ECW has also been successfully injected into the diverted plasma. The locked mode (LM), especially the 2/1 LM, is one of the biggest threats to the plasma operation, since it can lead to major disruption. It is hence important to study its formation and control. Both the thresholds of 2/1 and 3/1 LM are observed to vary non-monotonically on electron density. The electrode biasing (EB) was applied successfully to unlock the LM from either a rotating or static RMP field. In the presence of 2/1 LM, three kinds of standing wave (SW) structures have been observed to share a similar connection to the island structure, i.e. the nodes of the SWs locate around the O- or X- points of the 2/1 island. The control and mitigation of disruption is essential to the safe operation of ITER, and it has been systematically studied by applying RMP field, MGI and SPI on J-TEXT. When the RMP induced 2/1 LM is larger than a critical width, the MGI shutdown process can be significantly influenced. If the phase difference between the O-point of LM and the MGI valve is +90° (or -90°), the penetration depth and the assimilation of impurities can be enhanced (or suppressed) during the pre-TQ phase and result in a faster (or slower) thermal quench. During the MGI shutdown process, the runaway electron (RE) generation can be suppressed once n_e is larger than a critical threshold. This n_e threshold can be reduced by applying RMP field. A secondary MGI can also suppress the RE generation, if the additional high-Z impurity gas arrives at the plasma edge before TQ. When the secondary MGI has been applied after the formation of RE current plateau, the RE current can be dissipated, and the dissipation rate increases with the injected impurity quantity, but saturates with a maximum of 28 MA/s.

In the following two years, detailed researches with those newly developed diagnostics and auxiliary systems, e.g. ECE-imaging, VUV spectrometer, and Doppler reflectometry, will be beneficial for the study of MHD activities, turbulence and transport. The plasma operation with ECRH or poloidal divertor configuration will become more mature and it will inspire further researches on plasma heating, current drive, MHD and disruption control, boundary physics, etc.

ACKNOWLEDGEMENTS

This work is supported by the National MCF Energy R&D Program of China (Contract No. 2018YFE0309100, 2018YFE0310300), the National Key R&D Program of China (No. 2017YFE0302000) and the National Natural Science Foundation of China (Nos. 11675059, 11905078, 12075096, 12047526 and 51821005).

APPENDIX. THE J-TEXT TEAM

To be updated WRT v NF_2019.

REFERENCES

[1] Y. Liang *et al* 2019 *Nucl. Fusion* **59** 112016
[2] G. Zhuang *et al* 2011 *Nucl. Fusion* **51** 094020
[3] J.L. Zhang *et al* 2020 *IEEE Trans. Plasma Sci.* **48** 1560
[4] Y.Z. Tian *et al* 2019 *Fusion Eng. Des.* **146 A** 269
[5] Z. Wang *et al* 2021 *IEEE Trans. Plasma Sci.* **49** 258
[6] P. Edmonds *et al* 1989 *Fusion technology* **1**
[7] X. Xie *et al* 2014 *Nuclear Fusion and Plasma Physics* **34** 80
[8] Z.P. Chen *et al* 2016 *Rev. Sci. Instrum.* **87** 11D408
[9] M. Xia *et al* 2019 *Fusion Eng. Des.* **146** 578
[10] Z.P. Chen, *this conference*, P5-1199
[11] X.L. Xie *et al* 2020 *Fusion Eng. Des.* **155** 111636
[12] X.M. Pan *et al* 2016 *Rev. Sci. Instrum.* **87** 11E10611
[13] Z.J. Yang *et al* 2020 *Fusion Eng. Des.* **153** 111494
[14] X.H. Ren *et al* 2021 *Rev. Sci. Instrum.* **92** 033545
[15] X.Y. Zhang *et al* Upgrade of Vacuum Ultraviolet Spectroscopy System on J-TEXT, *Rev. Sci. Instrum.* (submitted)
[16] Z. Huang *et al* 2020 *Nucl. Fusion* **60** 064003
[17] D. Li *et al* 2020 *Nucl. Fusion* **60** 056022
[18] Z.P. Chen *et al* 2021 *Nucl. Fusion* **61** 02600
[19] N.C. Wang *et al* 2019 *Nucl. Fusion* **59** 026010
[20] L.Z. Liu *et al* 2019 *Nucl. Fusion* **59** 126022
[21] N.C. Wang *et al* Observation of a 3 kHz standing wave in the presence of the quasi-static magnetic island on J-TEXT. *47th EPS Plasma Physics conference* (June 21-25, 2021)
[22] N.C. Wang *et al* 2014 *Nucl. Fusion* **55** 064014
[23] R. Buttery *et al* 1999 *Nucl. Fusion* **39** 1827
[24] H.H. Wang *et al* 2018 *Nucl. Fusion* **58** 056024
[25] J.K. Park, N.C. Logan, MDC-19 Updates for ITER Error Field Correction Criteria. *34th meeting of the ITPA Topical Group on MHD Disruption and Control* (Garching, Germany, 14-17 Oct. 2019)
[26] W. Yan *et al* 2018 *Plasma Phys. Control. Fusion* **60** 035007
[27] Q. Hu *et al* 2016 *Nucl. Fusion* **56** 092009
[28] N.C. Wang *et al* Formation and control of the 3/1 locked island in the plasma boundary on J-TEXT. *10th International workshop on "Stochasticity in Fusion Plasmas (SFP)"* (Wuhan, China, 12 - 15 July 2021)
[29] J.C. Li *et al* 2020 *Nucl. Fusion* **60** 126002
[30] Y. Liang *et al* 2007 *Nucl. Fusion* **47** L21
[31] H. Liu *et al* 2017 *Nucl. Fusion* **57** 016003
[32] W. Jin *et al* 2013 *Plasma Phys. Controlled Fusion* **55** 035010
[33] P. Buratti *et al* 2005 *Nucl. Fusion* **45** 1446
[34] L.Z. Liu *et al* 2015 *Plasma Phys. Control. Fusion* **57** 065007
[35] M. Xu *et al* 2021 *Nucl. Fusion* **61** 036034
[36] Y.N. Wei *et al* 2019 *Plasma Phys. Control. Fusion* **61** 084003
[37] Z.F. Lin *et al* 2020 *Plasma Phys. Control. Fusion* **62** 025025
[38] R.H. Tong *et al* 2019 *Nucl. Fusion* **59** 106027
[39] Z.H. Jiang *et al* 2019 *Phys. Plasmas* **26** 062508
[40] C.H. Li *et al* 2020 *Plasma Phys. Control. Fusion* **62** 095010
[41] N.H. Cai *et al* 2021 *Fusion Eng. Des.* **169** 112488
[42] M. Zhang *et al* 2019 *Fusion Eng. Des.* **146** 1117
[43] Y.N. Wei *et al* 2020 *Plasma Phys. Control. Fusion* **62** 025002
[44] A.J. Dai *et al* 2018 *Plasma Phys. Control. Fusion* **60** 055003
[45] J. Hu *et al* 2020 *Plasma Sci. Technol.* **22** 115102
[46] Z.Y. Chen *et al this conference*, P5-1202
[47] Z.Y. Chen *et al* 2016 *Nucl. Fusion* **56** 074001
[48] Z.F. Lin *et al* 2019 *Plasma Phys. Control. Fusion* **61** 024005
[49] Y.J. Shi *et al* 2018 *Nucl. Fusion* **58** 044002
[50] Y.J. Shi *et al* 2020 *Nucl. Fusion* **60** 064002
[51] Z.J. Yang *et al* Observation of the electron thermal transport and temperature fluctuations for electron cyclotron heating plasma on J-TEXT, *Nucl. Fusion* (submitted)
[52] W. He *et al* 2019 *Plasma Phys. Control. Fusion* **61** 115016
[53] S.T Peng *et al* 2017 *Nucl. Fusion* **57** 036003
[54] L. Wang *et al* 2018 *Plasma Sci. Technol.* **20** 074004
[55] H.T. Huang and L. Wang 2020 *Plasma Sci. Technol.* **22** 105101
[56] S Taimourzadeh *et al* 2019 *Nucl. Fusion* **59** 046005
[57] N. D'Angelo 1965 *Phys. Fluids* **8** 1748
[58] P.J. Catto 1973 *Phys. Fluids* **16** 1719
[59] W.X. Guo *et al* 2019 *Nucl. Fusion* **59** 076012.
[60] A. Hasegawa and M. Wakatani 1987 *Phys. Rev. Lett.* **59** 1581
[61] W.X. Guo *et al* 2019 *Plasma Phys. Control. Fusion* **61** 105002